ISSN 0036-0244, Russian Journal of Physical Chemistry A, 2009, Vol. 83, No. 10, pp. 1682–1688. © Pleiades Publishing, Ltd., 2009.
Original Russian Text © I.K. Razumov, 2009, published in Zhurnal Fizicheskoi Khimii, 2009, Vol. 83, No. 10, pp. 1865–1871.

CHEMICAL THERMODYNAMICS AND THERMOCHEMISTRY

The Simulation of the Growth of Colonies in the Spinodal Decomposition of Metastable Phases

I. K. Razumov
e-mail: iraz@k66.ru
Received June 2, 2008

Abstract—The generalized continual hole gas model and Monte Carlo simulations were used to study the growth of colonies and lamellar segregations in the decomposition of metastable phases. The morphology of segregations qualitatively changed as the temperature decreased and depended substantially on the initial state (the presence of grain boundaries and critical equilibrium phase nuclei). The simulation results were compared with the kinetics of growth of eutectic colonies and morphologies of the decomposition of metastable austenite.

DOI: 10.1134/S0036024409100094

INTRODUCTION

Metastable phases corresponding to local minima of the Gibbs energy of an alloy have long been outside the scope of theoretical analysis. Classic thermodynamics does not consider metastable states because they are absent in equilibrium phase diagrams. The theory of spinodal decompositions [1] studies the morphology of segregations for simple models, where metastable phases cannot appear. Intermediate ordered states caused by the competition of ordering and decomposition processes at a long-range interatomic interaction potential were for the first time analyzed in [2] with the use of the Onsager semiphenomenological equations; the results were slightly different from those obtained in Monte Carlo simulations [3]. More recently, works that could be considered a development of Chen–Khachaturyan's ideas [2] were published [4, 5]. However, kinetics of the decomposition of a metastable phases is low investigated.

At the same time, studies of metastable phases is a problem of current interest [6]. First, it is not always clear which phases are stable and which metastable among intermetallic compounds [7]; the latter can decompose when diffusion is accelerated, e.g., under irradiation or intense plastic strain conditions [8]. Intermediate ordered states were, in particular, observed in Al–Mn [9], Fe–Co [10], Ni–V [11], Pt–V [7], Ti–V [3], Al–Fe [12], etc. alloys. Secondly, microstructures with a regular morphology of segregations can form in the decomposition of metastable phases; these microstructures impart special properties (strength, plasticity, etc.) to alloys. Transitions of this type are eutectoid decompositions of Cd–Sn, Ti–Mn, Ti–Cr, and Ti–Ni alloys [13]. The decomposition of metastable austenite (a disordered insertion solid solution of carbon in face-centered cubic Fe) accompanied by the growth of spherulitic colonies, which changes the properties of construction steels, is of special interest [14, 15].

In [16], diffusion equations were used to study the decomposition of a metastable ordered phase induced by a grain boundary. It was shown that a local decrease in the energy of ordering close to the boundary caused the formation of a chain of equally spaced segregations of equilibrium phases, which with time grew into the volume in the form of equally wide bands. In this work, we more thoroughly study the kinetics of growth of colonies, both from a grain boundary and from critical nuclei in volume, using this model and Monte Carlo simulations. The results obtained using the continual model and Monte Carlo simulations are compared with the kinetics of growth of eutectic [17, 18] and eutectoid [14, 15] colonies.

THE DECOMPOSITION OF A METASTABLE PHASE IN THE CONTINUAL MODEL

Model Formulation

In the thermodynamics of alloys [19], the form of the phase diagram is determined by the dependence of the Gibbs energy of mixing $f(C_A, T)$ on composition and temperature. In the model of regular solutions in the approximation of nearest-neighbor interactions, $f(C_A, T)$ is written as

$$f(C_A, T)/kT = (\Psi/2)C_A C_B + \sum_\sigma C_\sigma \ln C_\sigma, \quad \sigma = A, B, \tag{1}$$

where $\Psi = Z(2\varphi_{AB} - \varphi_{AA} - \varphi_{BB})/(kT)$ is the dimensionless energy of mixing, $\varphi_{\sigma\sigma'}$ denotes interatomic interaction potentials, Z is the coordination number, and $C_A + C_B = 1$. In this model, decomposition into

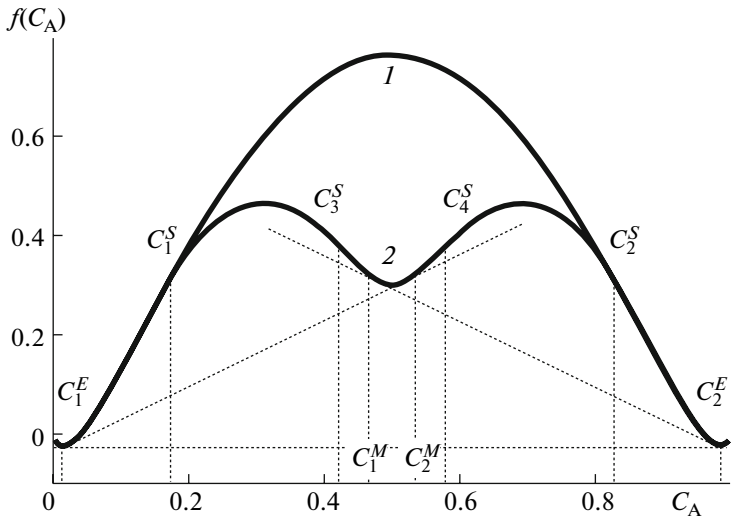

Fig. 1. Gibbs energy of mixing of alloy at $\Psi = 8.6$; $\Xi = (1)$ 0 and (2) 5; $C^E_{1,2}$ and $C^M_{1,2}$ are the limits of the main and metastable equilibria; $C^S_{1,2,3,4}$ denotes spinodes.

phases depleted of and enriched in one of the components occurs if $\Psi > 4$. At a fixed temperature, the decomposition is activationless within the convex portion of the $f(C_A)$ curve (Fig. 1, curve *1*); the inflection points C_1^S and C_2^S are called spinodes and determine the conditions of alloy stability loss. The equilibrium solubility limits C_1^E and C_2^E are determined by the common tangent to concave $f(C_A)$ curve portions as the abscissas of the tangency points.

At long-range potentials, the behavior of a system can change substantially; in particular, the difference between interatomic interaction energies for various coordination spheres can cause the formation of metastable ordered phases [2]. We restrict our consideration to the simplest case of ordering of the B2 type. In the mean-field approximation, the enthalpy per atom is then

$$H = \sum_{\sigma, n} E_\sigma^{(n)} C_\sigma^{(n)}/4,$$

where $C_\sigma^{(n)}$ and $E_\sigma^{(n)}$ are the concentrations and interatomic bond energies of atoms of kinds A and B in sublattices $n = 1, 2$. Bond energies are calculated by summing interaction energies with "own" and "foreign" sublattice atoms over the whole volume,

$$E_\sigma^{(n)}(\mathbf{r}) = \sum_{\sigma' = A, B} \sum_{i, m} \varphi_{\sigma\sigma'}^{(nm)}(\mathbf{q}_i) C_{\sigma'}^{(m)}(\mathbf{r} + \mathbf{q}_i). \qquad (2)$$

Since the $\varphi_{\sigma\sigma'}^{(nm)}$ potentials decrease rapidly as the distance increases, we, following [19], obtain $f(C_A, T)$ in the zeroth order of the expansion in $\mathbf{q}_i$ in the form

$$2f(C_A, T)/kT = \Xi\eta_A\eta_B + \Psi C_A C_B + \sum_{\sigma, n} C_\sigma^{(n)} \ln C_\sigma^{(n)}, \quad (3)$$

where $\eta_\sigma = (C_\sigma^{(1)} - C_\sigma^{(2)})/2$ and $C_\sigma = (C_\sigma^{(1)} + C_\sigma^{(2)})/2$. The dimensionless energies of mixing and ordering, Ψ and Ξ, are determined by the sum and difference, respectively, of the sublattice mixing energies χ^0 and χ^+ divided by the thermal energy kT,

$$\Psi = (\chi^0 + \chi^+)/kT, \quad \Xi = (\chi^0 - \chi^+)/kT,$$

$$\chi^{0(+)} = 2\Phi_{AB}^{0(+)} - \Phi_{AA}^{0(+)} - \Phi_{BB}^{0(+)},$$

$$\Phi_{\sigma\sigma'}^0 = \sum_i \varphi_{\sigma\sigma'}^{(nn)}(\mathbf{q}_i), \quad \Phi_{\sigma\sigma'}^+ = \sum_i \varphi_{\sigma\sigma'}^{(nm)}(\mathbf{q}_i), \quad m \neq n.$$

The degree of ordering η_σ can be calculated by the Bragg–Williams equation [20]

$$\frac{(C_\sigma - \eta_\sigma)(1 - C_\sigma - \eta_\sigma)}{(C_\sigma + \eta_\sigma)(1 - C_\sigma + \eta_\sigma)} = \exp[-2\Xi\eta_\sigma]. \qquad (4)$$

If $\Psi > \Xi > 4$, the $f(C_A)$ function has a local minimum at $C_A = 0.5$ corresponding to a metastable ordered state (Fig. 1, curve *2*). This minimum is responsible for the appearance of metastable solubility limits C_1^M and C_2^M and additional spinodes C_3^S and C_4^S.

A phase diagram calculated by (3) and (4) is shown in Fig. 2. Solid lines correspond to phase equilibrium conditions, and dashed lines, to alloy stability loss. The second spinodal lies above the metastable equilibrium curve, which results in qualitatively different decomposition kinetics in regions *1* and *2*.

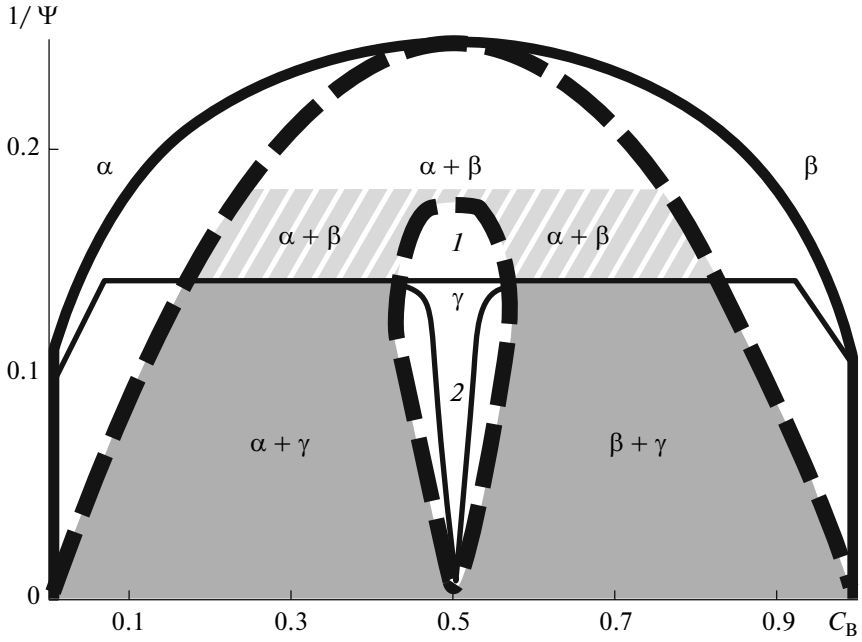

Fig. 2. Metastable phase diagram of an alloy with a tendency toward ordering ($\Psi = 1.2\Xi$); (*1*) region of autocatalytic decomposition (colonies) and (*2*) region of metastable equilibrium.

A microscopic formulation of decomposition kinetics equations corresponding to approximate thermodynamic equations (3) and (4) was suggested in [16]; it was a generalization of the hole gas method [21] to alloys with a tendency toward ordering. The model uses the main kinetic equation in the mean-field approximation for a system with the vacancy exchange mechanism as initial,

$$\frac{dC_\sigma^{(n)}}{dt}(\mathbf{r}) = \sum_{l=1}^{Z} \omega_\sigma^{(m)}(\mathbf{r}+\mathbf{a}_l \longrightarrow \mathbf{r}) C_V^{(n)}(\mathbf{r}) C_\sigma^{(m)}(\mathbf{r}+\mathbf{a}_l) - \omega_\sigma^{(n)}(\mathbf{r} \longrightarrow \mathbf{r}+\mathbf{a}_l) C_V^{(m)}(\mathbf{r}+\mathbf{a}_l) C_\sigma^{(n)}(\mathbf{r}), \quad (5)$$

where $C_A^{(n)} + C_B^{(n)} + C_V^{(n)} = 1$, $C_V^{(n)}$ is the concentration of vacancies in sublattice n, $C_V^{(n)} \ll C_\sigma^{(n)}$, and $\mathbf{a}_l$ denotes radius vectors of the nearest neighbors of the distinguished node $\mathbf{r}$. The frequencies of jumps are determined by the equalities

$$\omega_\sigma^{(m)}(\mathbf{r}+\mathbf{a}_l \longrightarrow \mathbf{r}) = \omega_{\sigma 0} \exp\left[(E_\sigma^{(m)}(\mathbf{r}+\mathbf{a}_l) - E_\sigma^S)/kT\right],$$

$$\omega_\sigma^{(n)}(\mathbf{r} \longrightarrow \mathbf{r}+\mathbf{a}_l) = \omega_{\sigma 0} \exp\left[(E_\sigma^{(n)}(\mathbf{r}) - E_\sigma^S)/kT\right].$$

Equation (5) is in essence the substance balance equation: a change (per unit time) in the probability of finding an atom of kind $\sigma = A, B$ at node $\mathbf{r}$ is the sum of the probabilities of transfer of atoms of this kind from all the nearest environment nodes into the given node less back transfer probabilities. The energy of an atom at saddle point E_σ^S is assumed to be constant. The approximations of local equilibrium ordering, local equilibrium of vacancies, and smooth changes in concentrations at distances on the order of the lattice parameter can be used to rewrite (5) as [16]

$$\frac{dC_A}{dt} = -\nabla \mathbf{J}_A,$$
$$\mathbf{J}_A = M\nabla\left[\ln\left(\frac{C_B^{(1)}}{C_A^{(1)}}\right) + \frac{(E_B^{(1)} - E_A^{(1)})}{kT}\right], \quad (6)$$

where M is the generalized mobility depending on diffusion mobilities and the concentrations of atoms and vacancies in sublattices. To describe the evolution of concentrations in the region of interphase boundaries, second-order terms should be retained in bond energy expansions (2) in $\boldsymbol{q}_i$ (first-order terms are absent because of lattice symmetry),

$$E_\sigma^{(n)}(\mathbf{r}) = \sum_{\sigma' = A, B} \Phi_{\sigma\sigma'}^0 (C_{\sigma'}^{(n)} + R^2 \Delta C_{\sigma'}^{(n)}) + \Phi_{\sigma\sigma'}^+ (C_{\sigma'}^{(m)} + R^2 \Delta C_{\sigma'}^{(m)}), \quad m \neq n.$$

The small parameter R having the meaning of the effective interatomic interaction radius is assumed to be constant.

Numerical Solution

Equation (6) was solved numerically by the standard Runge–Kutta method in an $L \times L$ $2D$ region ($L = 100R$) on the assumption that atomic fluxes through square boundaries were absent.

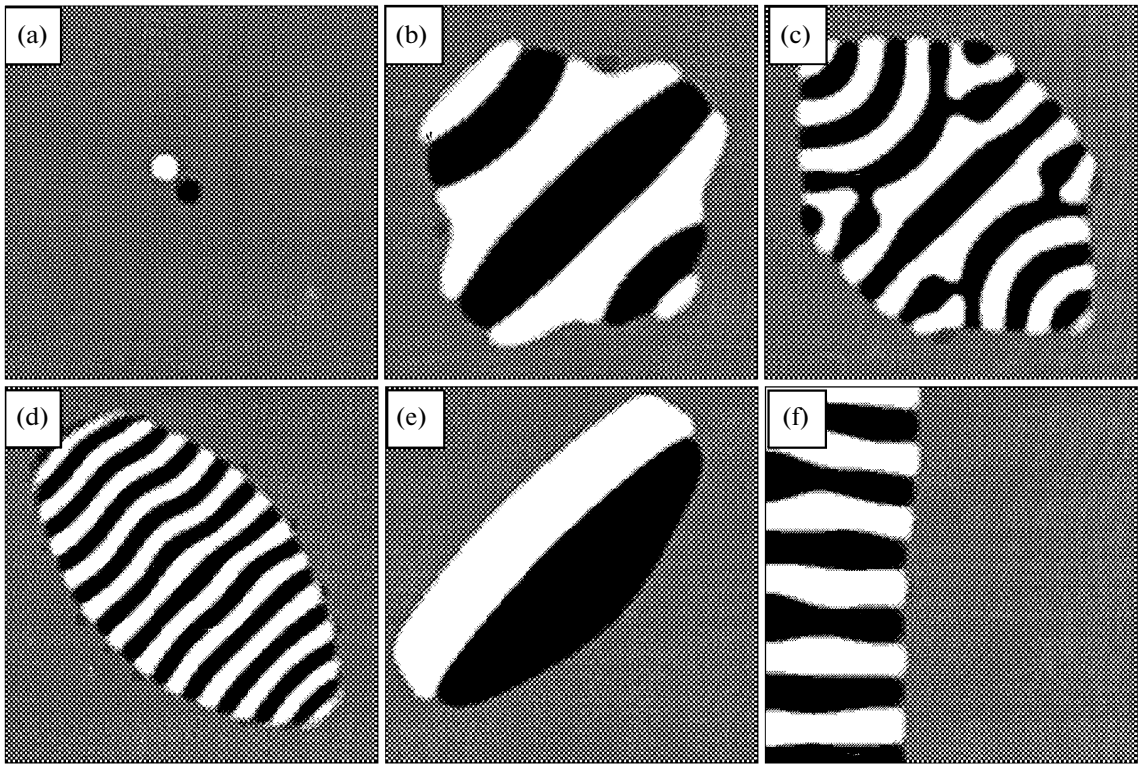

Fig. 3. Characteristic morphologies of segregations formed in the decomposition of a metastable phase; (a) initial state common to (b–e); Ψ/Ξ = (b, c, e, f) 1.2 and (d) 1.5; Ψ = (b, f) 6, (c) 6.6, (d) 7.8, and (e) 7.2; (f) decomposition induced by a decrease in the energy of ordering Ξ by 50% in the border region $2R$ wide.

In calculations presented in Figs. 3b–3e, the initial state was ordered (γ) with small Gauss composition fluctuations and two touching nuclei of the α and β phases (Fig. 3a). In real systems, such nuclei can appear spontaneously, especially close to lattice defects. The mean composition was close to equiatomic, and the temperature was fairly low. Alloy parameters were therefore in region *1* or *2* of the phase diagram (Fig. 2), where the initial state in the absence of critical perturbations remained uniform and ordered indefinitely long. Phases depleted of and enriched in component *A* are shown by white and black, and the ordered state, by gray in Fig. 3.

In phase diagram region *1*, decomposition develops autocatalytically, and the segregation of each phase causes the appearance of segregations of the other phase in its neighborhood. As a result, a colony consisting of lamellas with approximately equal widths λ is formed. The lamellas slowly evolve to decomposition. The dependence of λ on temperature and the Ψ/Ξ ratio is complex in character. For instance, at Ψ/Ξ = 1.2, λ increases as the temperature grows (compare Figs. 3b and 3c). Calculations performed at $\Psi/\Xi = 1.5$, however, revealed a nonmonotonic $\lambda(T)$ dependence. In all instances, lamellas were initially oriented parallel to each other. In microstructures with $\lambda \gg R$ at later stages, we, however, observe the transition to dendritic growth (Fig. 3c). In narrow-band microstructures, the transformation front is stabler toward autocatalytic nucleation of new bands. A typical colony has an ellipsoidal shape and a regular structure (Fig. 3d). Decomposition can also be induced by one nucleus; the ring structure that appears at the initial stage then changes into dendritic growth.

Supercooling into region *2* of the phase diagram stops autocatalysis; a single nucleus remains at equilibrium with the γ phase, but a pair of touching nuclei develops into a double lamella (Fig. 3e). The thickness of the lamella increases indefinitely, but the rate of thickening decreases with time, whereas the rate of lamella elongation remains constant. This decomposition type can be called "needle-like."

It was shown in [16, 22] that grain boundaries play an important role in spinodal decomposition; close to grain boundaries, the thermodynamic properties of an alloy can change locally. In particular, a wave stage of spinodal decomposition develops as the energy of ordering decreases close to grain boundaries, and a chain of $\alpha$and β phase segregations is then formed. These segregations grow into grain volume with time (Fig. 3f) in the form of lamellas with equal widths. The formation of a regular structure of this type is possible in both regions *1* and *2* of the phase diagram, but, in region *2*, only at specially adjusted parameters (the width of the boundary region and the amplitude of perturbation). Lastly, if $\nabla\Psi \neq 0$ close to the grain

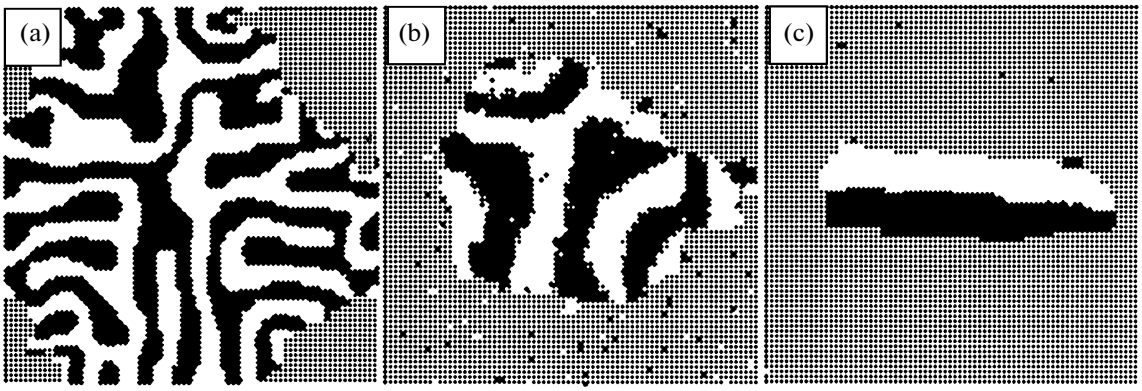

Fig. 4. Characteristic morphologies of segregations formed in the decomposition of a metastable phase, Monte Carlo simulation results; $\varphi_{AA}^{(1)}/\varphi_{AA}^{(2)}$ = (a) 0.25 and (b, c) 0.09; $-\varphi_{AA}^{(1)}/kT$ = (a) 0.5, (b) 0.083, and (c) 0.125.

boundary, uniform segregations that induce the decomposition of the γ phase without the formation of microstructures are formed.

The Simulation of Decomposition by the Monte Carlo Method

The kinetics of decomposition of an AB alloy with a body-centered cubic lattice was studied in a quasi-two-dimensional region (75 × 75 × 1 cells) with periodic boundary conditions by a method similar to that used in [23]. In this model (1) diffusion occurs by a vacancy jump into position $i = 1...Z$ of one of the neighboring atoms; (2) the probability of the jump is $\Gamma_\sigma^{(i)} \sim \exp[-\Delta E_\sigma^{(i)}/kT]$, σ = A, B, and the activation energy of the jump equals the difference between the energies of an atom at the saddle point and in the ground state ($\Delta E_\sigma^{(i)} = E_{i\sigma}^{S} - E_{i\sigma}^{(0)}$); the sum of the probabilities of all jumps at one simulation step is normalized to one (the BKL algorithm [24]); (3) the energy at the saddle point is assumed to be independent of configuration $E_{i\alpha}^{S} = E^{S} = \text{const}$, the energy in the ground state equals the sum of pair interaction energies over several coordination spheres ($E_{i\sigma}^{(0)} = \sum_{K,\sigma'} \varphi_{\sigma\sigma'}^{(K)} N_{\sigma'}^{(iK)}$, where $\varphi_{\sigma\sigma'}^{(k)}$ is the interaction energy between atoms of kinds σ and σ' removed by the distance of the Kth coordination sphere containing $N_{\sigma'}^{(iK)}$ atoms of kind σ'). The number of independent model parameters $\varphi_{\sigma\sigma'}^{(K)}$ was reduced to two ($\varphi_{AA}^{(K)} = \varphi_{BB}^{(K)}$, $\varphi_{AB}^{(K)} = 0$; $K = 1, 2$), which was sufficient for analyzing the general rules governing the decomposition of a metastable phase. Our model parameters are related to continual model parameters as $\Psi = -2[8\varphi_{AA}^{(1)} + 6\varphi_{AA}^{(2)}]/kT$; $\Xi = 2[8\varphi_{AA}^{(1)} - 6\varphi_{AA}^{(2)}]/kT$.

The characteristic morphologies of the decomposition of a metastable phase induced by the introduction of a pair of touching nuclei of the α and β phases into the initial state with the parameters corresponding to region *1* or *2* of the phase diagram (Fig. 2) are shown in Fig. 4. Atoms of kinds A and B are shown in black and white, respectively; image continuity was obtained by the superposition of two lattice layers. We see that the simulation results are qualitatively similar to the predictions of the continual model. At moderate temperatures, we observe autocatalysis of lamellas (Figs. 4a, 4b), the width of lamellas has a complex dependence on T and Ψ/Ξ, and the transition to needle decomposition is observed at low T (Fig. 4c). We were, however, unable to obtain a regular morphology of lamellas similar to that shown in Fig. 3d in Monte Carlo simulations; a typical colony had a radial-feathered structure (Fig. 4a). The conditions of the beginning of decomposition were slightly shifted to lower temperatures compared with the phase diagram of the continual model (Fig. 2). In addition, we can expect the nucleation of new bands for needle decomposition at long exposures because of thermal composition fluctuations.

RESULTS AND DISCUSSION

The model predicts the possibility of the decomposition of metastable ordered phases (Al–Mn, Ti–V, etc.) by the colony growth mechanism and can be useful for analyzing physically related phenomena, such as eutectic [17, 18] and eutectoid [14, 15] transformations. It was shown in [17, 18] that the growth front of a eutectic colony can experience instability; stationary growth is observed over an optimum range of λ values. It is also known from experiments that lamellas in ledeburite cylindrical colonies are oriented normally to the colony growth front [25] as in Figs. 3c, 4a.

Qualitative similarity of the phenomenon to the kinetics of metastable phase decomposition is caused by similar thermodynamic characteristics of the trans-

formations. In both cases, two thermodynamic factors compete. One of these provides homogeneous state stability toward small composition fluctuations, and the other contributes to decomposition into equilibrium phases, which decreases the Gibbs energy. In solidification, there is a temperature drop at the colony growth front, whereas in metastable ordered phase decomposition, the $f(c)$ local minimum is caused by the tendency toward ordering close to equiatomic composition.

The possibility of spontaneous formation of critical nuclei is not described by the continual model, but if α and β phase nuclei are introduced into the initial state, nonzero atom fluxes appear in the region of their contact, which results in the development of lamellas. Note that, in analyzing eutectic colonies, (1) the initial λ value was determined by the periodic distribution of concentrations at the boundary of the simulation region, and (2) the development of colonies from segregations in the volume was not considered, and the autocatalysis of lamellas was therefore only observed in their splitting under dendritic growth conditions.

The morphologies of segregations obtained in simulation were also similar to the decomposition of metastable austenite in steels [14, 15]. When austenite is annealed at temperatures of from 727 to 500°C, pearlite, sorbite, and troostite are sequentially formed with a decreasing incubation period. The thickness of lamellas decreases from 1 μm (pearlite) to 0.1 μm (troostite). Annealing below 500°C transformed austenite depleted of carbon into ferrite by the shear mechanism. At $350°C < T < 500°C$, upper bainite with a feathered microstructure, and, at $T < 350°C$, needle lower bainite were formed. Grain boundaries lead to independent morphologies known as polygonal and Widmansäatten ferrite; the latter is formed at elevated temperatures. We see that the suggested model taking into account the competition of two thermodynamic factors Ψ and Ξ gives a qualitatively similar picture of the growth of colonies and needle segregations, which is evidence of physical generality and prevalence of the phenomenon.

The model predicts the formation of regular pearlite-like (Figs. 3b, 3d) and dendritic (Fig. 3c) microstructures as the alloy is cooled into region *1* of the phase diagram. With $\Psi/\Xi = 1.2$, the interlamellar distance λ decreased as T lowered (compare Figs. 3b and 3c). The experimentally observed change of pearlite, sorbite, and troostite structures and the shape of colonies close to spherical are evidence of autocatalysis of lamellas, which is only possible in the absence of metastable equilibrium between austenite and decomposition products. A further decrease in T leads into phase diagram region *2*, where autocatalysis of lamellas stops and needle decomposition (Fig. 3e) similar to bainite transformation is observed. The difference between phase diagram regions *1* and *2* (the noncoincidence of spinodal vertices and metastable equilibrium curves) should be a common feature of many metastable systems with a local $f(c)$ minimum. Lamellas oriented normally to a grain boundary (Fig. 3f) are similar to Widmanstätten ferrite. The precipitation of a phase similar to polygonal ferrite on a grain boundary can be caused by grain boundary segregations.

As distinct from diffusion equations, Monte Carlo simulation takes into account spontaneous composition fluctuations, which results in less regular segregation morphologies compared with the continual model. It follows that regular pearlite colonies nucleate in a comparatively homogeneous medium, whereas strong heterogeneity distorts the regularity of lamellas. This conclusion is in agreement with the technology for the preparation of granular pearlite from an inhomogeneous state [15]. The results of Monte Carlo simulation and continual model should converge for long-range potentials, which can be obtained for particular systems from first-principles calculations [26].

To summarize, metastable phases experience decomposition by the mechanism of nucleation and growth of pearlite-like colonies or needle segregations from regions with disturbed homogeneity (grain boundaries and critical nuclei of equilibrium phases). The width of a lamella in colonies is determined by autocatalysis and depends on temperature and interatomic interaction parameters. Autocatalysis of lamellas exists over a limited temperature range. At low temperatures, critical composition fluctuations lead to needle decomposition.

ACKNOWLEDGMENTS

The author thanks director of ZAO "Institute of Quantum Materials Science" Professor Yu.N. Gornostyrev for instructive discussions.

REFERENCES

1. J. W. Cahn, Acta. Metall. **9**, 795 (1961).
2. L. Q. Chen and A. G. Khachaturyan, Phys. Rev. B **44**, 4681 (1991).
3. L. Reinhard and P. E. A. Turchi, Phys. Rev. Lett. **72**, 120 (1994).
4. Ni. Jun and Gu. Binglin, J. Phys.: Condens. Matter **10**, 3523 (1998).
5. Ni. Jun, T. Ashino, and S. Iwata, Acta Mater. **48**, 3193 (2000).
6. V. V. Brazhkin, Usp. Fiz. Nauk **176**, 745 (2006) [Phys. Usp. **49**, 719 (2006)].
7. *State Diagrams of Double Metallic Systems, The Manual*, in 3 vols., Ed. by N. P. Lyakishev (Mashinostroenie, Moscow, 2000) [in Russian].
8. A. E. Ermakov, Fiz. Met. Metalloved., No. 11, 4 (1991).
9. E. I. Teitel', M. A. Uimirn, A. E. Ermkakov, et al., Fiz.-Khim. Mekh. Mater., No. 8, 83 (1990).
10. T. G. Woodcock, R. Hermann, and W. Löser, CALPHAD: Comput. Coupling Phase Diagrams Thermochem. **31**, 256 (2007).

11. C. Notthoff, B. Feuerbacher, H. Franz, et al., Phys. Rev. B **86**, 1038 (2001).
12. H. Chen, J. Anderson, K. Ohshima, et al., Phys. Rev. Lett. **42**, 2342 (1990).
13. G. N. Dubinin, *Construction, Conducted, and Magnetic Materials (Electric Science of Materials)* (Nauka, Moscow, 1973) [in Russian].
14. V. M. Schastlivtsev, D. A. Mirzaev, I. L. Yakovleva, et al., *Pearlite in Carbon Steels* (Ural. Otd. Ross. Akad. Nauk, Yekaterinburg, 2006) [in Russian].
15. M. L. Bernshtein, G. V. Kurdyumov, V. S. Mes'kin, et al., *Science of Materials and Thermal Processing of Steel and Cast Iron, the Manual*, in 3 vols., Ed. by A. G. Rakhshtadt, L. M. Kaputkina, S. D. Proshkin, and A. V. Stupov (Intermet Eng., Moscow, 2005) [in Russian].
16. I. K. Razumov, Inzh.-Fiz. Zh. **81**, 789 (2008).
17. V. Datye and J. S. Langer, Phys. Rev. B **24**, 4155 (1981).
18. M. Apel, B. Boettger, H. J. Diepers, and I. Steinbach, J. Cryst. Growth **237–239**, 154 (2002).
19. J. Christian, *Theory of Transformations in Metals and Alloys* (Pergamon, Oxford, 1975; Mir, Moscow, 1978).
20. J.-F. Couet, M. Plapp, W. Dieterich, and P. Maass, Adv. Phys. **52**, 523 (2003).
21. *Processes of Mutual Diffusion in Alloys*, Ed. by K. P. Gurov (Nauka, Moscow, 1973) [in Russian].
22. I. K. Razumov, Yu. N. Gornostyrev, and A. Ye. Yermakov, J. Alloys Compd. **434–435**, 535 (2007).
23. F. Soisson, A. Bardu, and G. Martin, Acta Mater. **44**, 3789 (1996).
24. A. B. Bortz, M. H. Kalos, and J. L. Lebowitz, J. Comp. Phys. **17**, 10 (1975).
25. V. E. Ol'shanetskii, Metalloved. Term. Obrab. Met., No. 1, 6 (2008).
26. V. F. Rashnikov, A. A. Morozov, V. N. Urtsev, and Yu. N. Gornostyrev, Stal' **2**, 104 (2007).